SI Appendix

Precision, accuracy, and resolution for NuRIM

The precision σ is an estimate of the reproducibility of a measurement process as quantified by the standard deviation taken across multiple measures m1, m2, m3… of the same quantity. The accuracy (or "trueness") refers to the bias in those measurements, i.e. whether the mean M taken across a very large number of these measurements is equal to the "true" value T). Accuracy is measured by the difference: T-M.

If NuRIM measures positions equal to 30nm, 40nm, and 35 nm for a particular Nup in three separate experiments, the precision of those measurements is σ=5nm. The precision claimed for NuRIM was obtained by averaging the calculated precision obtained over 28 different Nups (σ=1.5 nm i.e. ~2 nm, see *SI*, Dataset S1 - Sheet1).

When we examine e.g. whether compositional plasticity is accompanied by structural plasticity, we need to decide whether the small changes observed in the positions of particular Nups are significant and this can only be done by comparing them to the precision of NuRIM, e.g. using the Student T test. Accordingly, a change is significant if its amplitude exceeds twice the precision (the p-value is then below 5%).

Precision only informs on reproducibility – not accuracy. In order to determine accuracy, one would ideally apply NuRIM to an object - the dimension T of which is known perfectly. This is easy to do in the case of simulations: it suffices to simulate a pair of nucleoporins with a position difference of e.g. 5 nm and to verify whether NuRIM can accurately recover that distance when applied to the corresponding set of simulated images. The process is then repeated for e.g. 3 different conditions of background fluorescence, thus producing pairwise differences T_1-M_1, T_2-M_2, T_3-M_3. Finally, those pairwise discrepancies are combined into a single accuracy measure: the pairwise root mean square difference (RMSD) as used throughout our text:

$$RMSD = \sqrt{\frac{(T_1 - M_1)^2 + (T_2 - M_2)^2 + (T_3 - M_3)^2}{3}}$$

Experimentally however, an object of exactly known dimensions T is not available. Therefore, we perform various experiments intimately related to the notion of accuracy. For example, most researchers would be so confident that NPCs exhibit the same structure in diploid and haploid strains that they would consider any discrepancy in the corresponding measurements to be a consequence of NuRIM's inaccuracy. More precisely, they would use a particular dimension obtained on the haploid strain as a reference yardstick of length T, which they can then compare to the corresponding dimension M measured in the diploid strain in order to compute (in)accuracy: T-M. We note that T was obtained experimentally so it is also subject to an imprecision σ, and so is M. Therefore, our reported measure of accuracy (~2 nm on average, see *Main Text*, Table 1) is conservative.

www.pnas.org/cgi/doi/10.1073/pnas.1903764116

Generative modeling of NPCs in the nuclear envelope

To establish a quantitative understanding of nuclear radial intensity measurements (NuRIM), we have relied on a generative 3D model of the nuclear envelope (NE) populated by NPCs (*Main text*, Fig. 2*A*). An earlier version of this model was presented and is reproduced here with several improvements (1). In budding yeast, NEs are approximately spherical with a mean average radius of 1.0 μm and they were modeled as spheres of that size (2). NPCs were distributed randomly on the surface of the sphere. Further, it was observed by Winey *et al.* that the nearest neighbor distribution between NPCs displays an exclusion zone of approximately 200 nm, presumably due to steric effects between NPCs (2). To replicate the cumulative nearest distance distributions, we used ancestral sampling - rejecting new NPC instances that would lie closer than that cutoff and until a total of 120 NPCs on average were produced. The value of 120 NPCs per nucleus was also obtained from the work of Winey *et al.* In order to simulate the reference dsRed-HDEL channel, a random distribution of one thousand dim probes induced a more continuous signal at the NE. Finally, nuclei do not lie systematically at the center of cells, so randomization was also introduced here (Fig. S1C).

To produce sample images of NEs, simulated NEs in the object space were convoluted using a realistic point spread function (PSF) computed using the code from Pankajakshan *et al.* (3). A computed PSF was used rather than an experimental PSF because it is not trivial to obtain a fully satisfactory PSF experimentally. The computed PSF was then convolved with our simulated data. This process yielded realistic images of NEs, such that it was difficult to distinguish synthetic images from genuine ones. In order to take into account that nuclei may lie anywhere within cells during imaging, a slice was selected randomly from the 10 slices closest to the brightest one.

Our model was used to investigate the influence of several factors that may affect the measurement process, including nuclear/cytoplasmic background fluorescence and intensity at the NE, projection from 3D to 2D, and chromatic aberrations. To achieve this, NuRIM was applied to the simulated images, exactly as for actual images, but with full knowledge of the ground truth.

Compared to the code presented earlier (1), this version (*SI*, Dataset S2) includes a better method to identify NEs (4), random positioning of NEs within cells, more realistic modelling of the camera and photon noise following the approach of Dignam *et al.* (5), as well as independent control of the fluorescence levels in the NE, the nucleus, and the cytoplasm (Fig. S1).

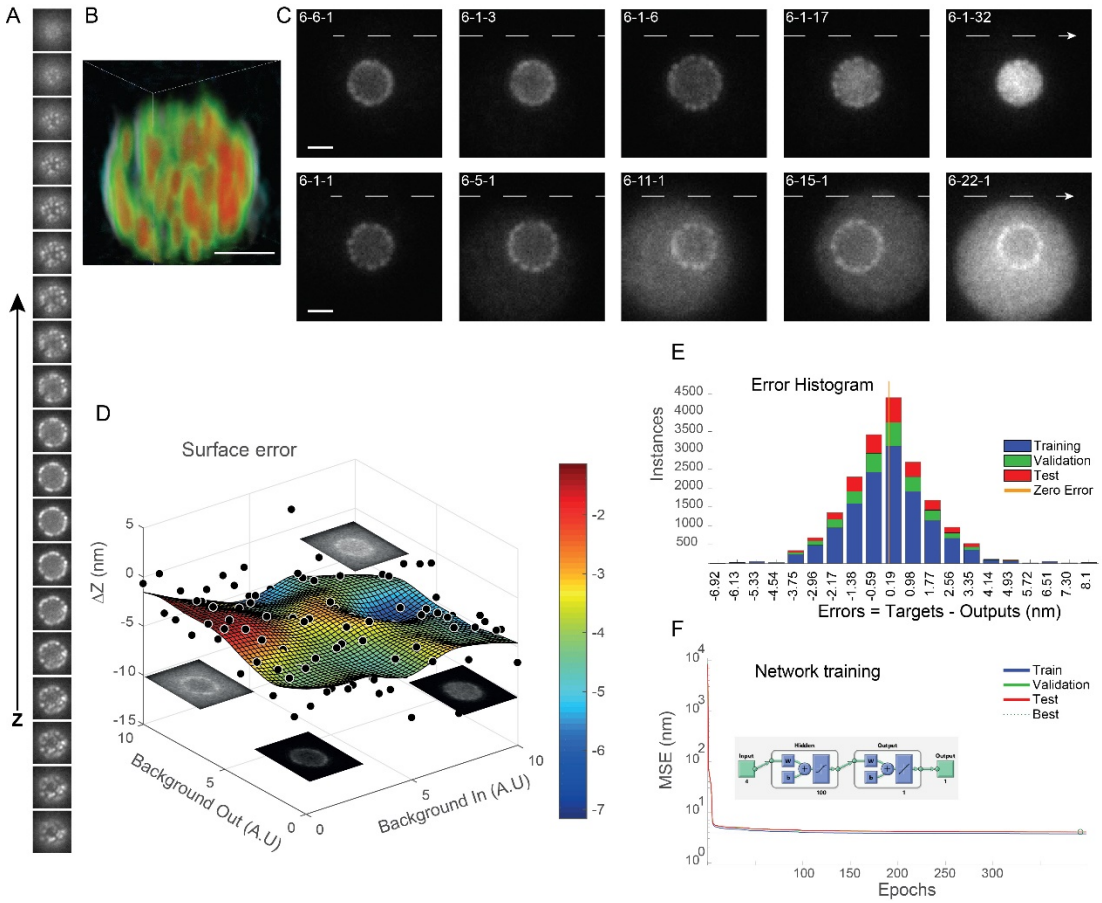

Fig. S1. NE simulations and bias removal using machine learning. (*A*) Over 160'000 artificial images, each sampled from independent 4D volumes 200x200x200x2 voxels in size, were produced and analyzed using NuRIM (successive slices corresponding to a single volume are shown). Thus, bias errors ΔZ associated with the method could be assessed in a wide range of conditions and with full knowledge of the ground truth. These errors may then be used to systematically adjust experimental position measurements in given conditions of signal at the NE and background fluorescence in the nucleus and cytoplasm. (*B*) 3D volume rendering produced with ImageJ for the data shown in *A*. (*C*) Representative simulated images demonstrating the effect of varying NE intensities as well as cytoplasmic and background fluorescence levels (levels are indicated by the notation: Signal_NE - Background_Cyt - Background_Nucl). (*D*) Colored surface represents best-fit error obtained by training a neural network. Each black dot is a training point obtained by averaging across 64 simulated nuclei per condition (*E*) The Matlab plot shows the error that remains after the neural network has performed positional adjustments. (*F*) The time-course for convergence of the neural network training is also shown. Scale bar: 1μm

The NuRIM measurement process

The specification of the NuRIM method is given by the corresponding code (*SI*, Dataset S3). NuRIM measures radial shifts between the yEGFP-tagged nucleoporin (Nup) of interest and a reference protein (e.g. dsRed-HDEL) that provides a fiduciary marker at the NE. The two signals are spectrally distinct and acquired using appropriate microscope filter cubes for yEGFP and dsRed respectively, thus avoiding restrictions associated with the Abbe limit (6). Any crosstalk between channels will negatively affect the results. Therefore, suitability of the filters should be checked by imaging yEGFP using the dsRed channel, and vice versa. Crosstalk would lead to an artificial compression of the distances measured by NuRIM.

Our implementation draws digital lines from the nucleus center of mass, outwards across the NE. The pixel intensities along these lines in the reference channel display a local maximum at the level of the NE (*Main text*, Fig. 1). Super-resolution emerges because thousands of such intensity profiles are analyzed, thus averaging out random variations that are not directly related to underlying structural shifts. Using the Matlab™ parallel computing toolbox on a cluster of 64 cores, it was possible to process ~20 images per minute, compared to ~1 image per minute for a single core.

In order to maximize the number of profiles available for the analysis, we used a sensitive nucleus detector as described by Hadjidemetriou *et al.* (4). Briefly, the method first identifies all edges in the image and then systematically traces normals to those edges. The intersections of those normals tend to occur at the center of nuclei. An important aspect of the method is the introduction of weight decay factors that are largest at the edges and decrease exponentially away from them – such that signals contributed by different cells interfere only minimally with each other.

NuRIM may be summarized by the following steps:

- The two image channels are first registered with high precision using the function "dftregistration.m" contributed by Manuel Guizar (7).
- Images are background-corrected using a top hat morphological filter.
- NEs are detected based on the fiduciary image channel, as described above (4)
- Only NEs corresponding to strict morphology selection criteria of size and shape are retained.
- The NE center of mass is computed
- Radial lines spanning 360° are generated
- Intensity profiles from both channels are sub-sampled along the radial lines by using spline interpolation
- The profiles are gated using binary masks produced by NuRIM in order to ensure that information remote from the NE cannot influence the outcome of the procedure (*Main text*, Fig. 1*E*)
- A Gaussian profile is fitted optimally on the radial profiles and if strict quality criteria of RMSD and full width at half maxima (FWHM) are met, the data for that particular ray are retained
- Shifts in position between the maxima associated with the two profiles are gathered and retained if they lie within 300 nm of each other.

- Results are pooled and averaged first on a cell by cell basis, then on an image by image basis. They are output to an excel file containing the following columns, with each row reporting the per-image averages:

  Filenames: Original name and location of the image file processed by NuRIM
  Average Intensity: Each NE contour corresponds to a one-pixel-wide closed curve. The average is first taken across all (background-corrected) pixel values of the contours, then across all contours of the corresponding image.
  BackgroundNup inside: Measures the level of background signal inside the nucleus in the Nup channel. No background correction is performed. The value is obtained based on a morphological erosion of the NE contours, 6 pixels away from the contour.
  BackgroundNup outside: Measures the level of background signal outside the nucleus in the Nup channel. No background correction is performed. The value is obtained based on a morphological dilation of the NE contours, 6 pixels away from the contour
  Radial [nm]: Position (i.e. height) of the nucleoporin relative to the reference NE marker used.
  Radial (adjusted) [nm]: The measurement of Nup position can be influenced by large levels of background fluorescence inside or outside nuclei. NuRIM includes a correction for such effects based on the measurement of Nup positions on simulated images spanning a wide range of imaging conditions (Fig. S1). Because the ground truth is known for simulated data (for example, the shift between test and reference protein may be set to 0 nm), a correction value may be obtained in each case and subtracted from each experimental value. Because the parameter space is quite large, a neural network was trained to deliver this correction on the basis of over hundred thousand training samples spanning a wide range of signal conditions. The Matlab neural network toolbox was used to train a network of 25 neurons using Levenberg-Marquardt minimization (Fig. S1). The training set was augmented by assuming invariance to scaling of intensities in the range 0.9-1.1. The biases were less than 5 nm for most Nups (*SI*, Dataset S1- Sheet 1).

NuRIM provides high accuracy because it is a "differential" method.

To see what is differential about NuRIM, assume that dsRed-HDEL stands on average δ nanometers above the NE (taken as zero height), and that one wishes to determine the relative elevation of Nup60-yEGFP versus Nup159-yEGFP within the NPC structure. In a first sub-experiment, one would measure $h_{60} - \delta$ for the height of Nup60-yEGFP relative to the reference dsRed-HDEL probe, and in a separate sub-experiment, one would measure $h_{159} - \delta$ for the height of Nup159-yEGFP relative to dsRed-HDEL. We can then deduce that Nup159-yEGFP lies above Nup60-yEGFP by an amount equal to $(h_{159}-\delta)-(h_{60}-\delta) = h_{159}-h_{60}$: the important point being that δ cancels out exactly, thus making the method "differential". It is understood that δ may be affected by additional sources of error associated with chromatic effects, time-delay effects, geometry effects, and other poorly characterized effects. However, these effects are expected to be present to the same extent in both sub-experiments, and thus cancel differentially to yield a highly precise value. The rest of this text is nonetheless aimed at characterizing those effects in more detail.

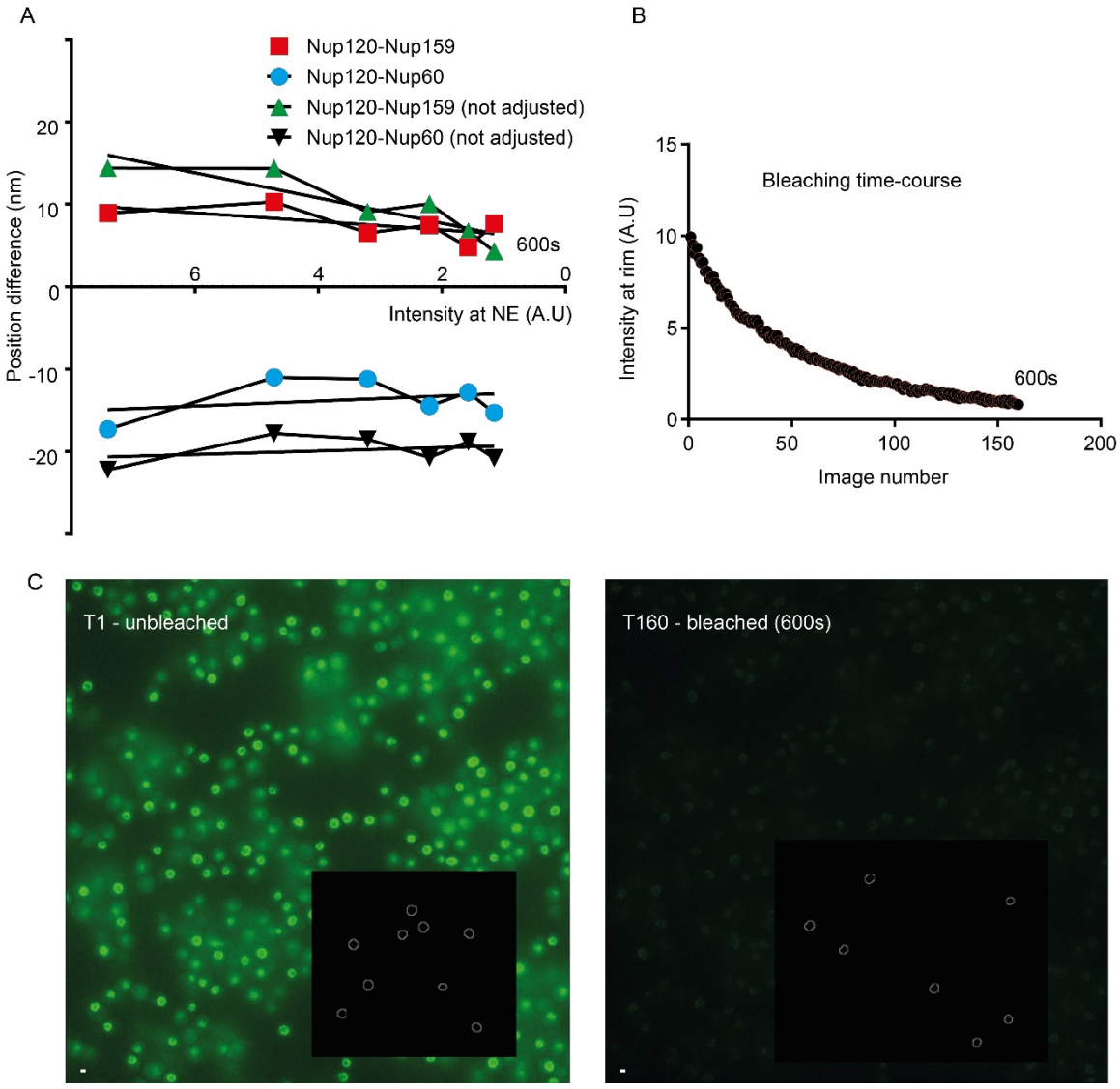

Fig. S2. Robustness of NuRIM measurement against photo-bleaching. (*A*) Position differences between Nup120-yEGFP and Nup60-yEGFP (resp. Nup120-yEGFP and Nup159-yEGFP) were measured over a period of 10 minutes during which the signal decreased by a decade (Illumination intensity was set to 100%). Position differences were stable in spite of considerable signal reduction. (*B*) Time-course of intensity for Nup120-yEGFP. (*C*) Corresponding images under identical contrast settings illustrates the extent of photo-bleaching. Inset show representative segmentation masks. Scale bar: 1μm.

Influence of the nuclear envelope size

In an interesting study, Wang *et al.* fitted the shape of the NE using splines to measure the average distance of a subset of Nups from the nucleus center (8). Small changes in nuclear diameter were interpreted as differences in Nup positions. Unfortunately, labelling particular Nups may affect NE diameter (Fig. S3) and even changes of a few percent can translate into shifts of tens of nanometers, thus rendering structural interpretations difficult. A core element of NuRIM is the implementation of a differential scheme that places this type of effects under tight control.

As an illustration, we noted that the nuclear size of the Nup57-yEGFP strain was larger than that of the majority of other strains (Fig. S3). Using NuRIM on more than a thousand nuclei, an apparent nuclear diameter of 1.89 ± 0.3 μm was determined for the Nup57-yEGFP strain, compared to only 1.54 ± 0.3 μm for the Nup84-yEGFP strain. But in spite of this difference of several hundred nanometers, positions determined by our method differed by less than 2 nm for these "symmetric" Nups (-0.1 ± 4.2 nm for Nu57-yEGFP, versus 1.7 ± 0.9 nm for Nup84-yEGFP, respectively). One should view changes in nuclear diameter as an indication of tag interference. For this reason, Nup57-yEGFP is marked with an * in Fig. 4*A* and the result is only provided for completeness.

We conclude that differential position measurements are highly precise, even in the presence of confounding variations in nuclear diameter.

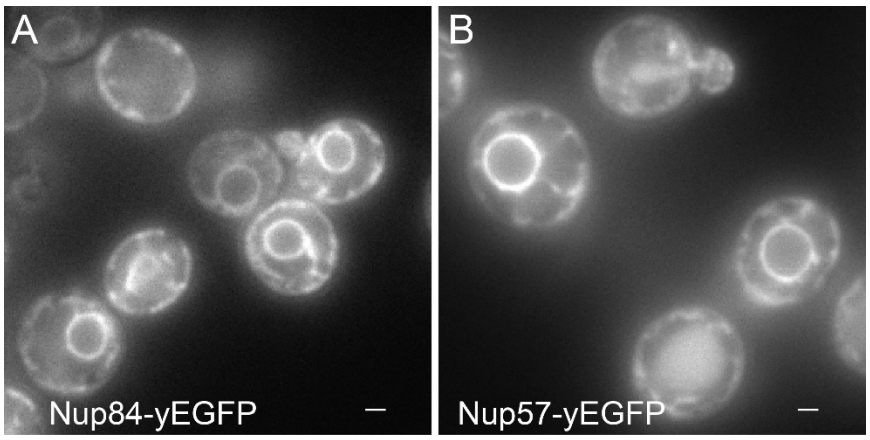

Fig. S3. Endogenous labelling may exceptionally lead to changes in nuclear diameter. (A) Image of a Nup84-yEGFP strain shown for comparison (dsRed-HDEL channel is shown). (B) Image of Nup57-yEGFP strain showing enlarged nuclei (dsRed-HDEL channel is shown). Accurate measurements may still be obtained by NuRIM, in contrast to methods that would directly rely on nuclear diameter measurements to infer structural information. Scale bars: 1μm.

Influence of chromatic aberrations and small acquisition delays between channels

Chromatic aberrations in fluorescence microscopy are the consequence of wavelength-dependent dispersion through the optics. They manifest themselves as a position-dependent shift of up to several pixels depending on the image channel selected. Because these shifts may be larger in magnitude than the NPC structure-related shifts that we aim to measure, they could possibly interfere with the methodology. We evaluated the magnitude of these effects by artificially translating one image channel versus the other by 1 to 3 pixels and comparing NuRIM measurements to the situation where no such shifts were performed. These experiments resulted in biases equal to 5.6 nm for a 1 pixel shift, 10.2 nm for a two-pixel shift, and 11.2 nm for a three-pixel shift, respectively. We thus introduced a sub-pixel accuracy channel alignment step in NuRIM based on the function 'dftregistration.m' contributed by Manuel Guizar, such that channel mis-registration does not cause significant biases in the production version (*SI*, Dataset S1; measured biases after registration were: -0.8nm, 0.6, and 0.2nm for shift equal to 1, 2, and 3 pixels, respectively). Chromatic effects may be subtler than global shifts. For example, the PSFs for different colors are slightly different, leading to e.g. different depths of field for different image channels. In order to evaluate the amplitude of such effects, we imaged the double mutant Sec61-yEGFP Sec61-mCherry as one would expect that the two proteins share the same sub-cellular localization. Using NuRIM, we measured a shift of 2.8+-11.3 (*SI*, Dataset S1).

We also probed the influence of the time delay in measuring one channel versus the other. This delay could potentially result in shifts in position similar to - but independent of those induced by chromatic aberrations. Thus, dsRed-HDEL was measured against itself with a time delay of 2 s - longer to that which was used under normal operations (0.5 s exposure was normally used). This experiment resulted in a shift of 1.2 ± 2.1 nm (*SI*, Dataset S1).

We stress again that because NuRIM is a differential method, most of the effects described in this appendix are expected to cancel out when performing structural measurements using the recommended methodology.

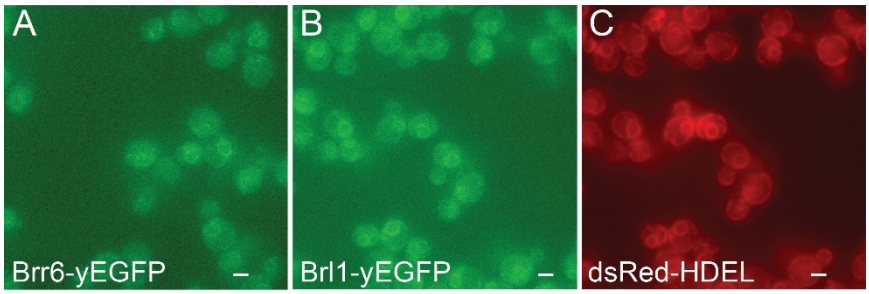

Fig. S4. NuRIM is widely applicable to characterize the spatial distribution of NE-associated biomolecules. For example, it was applied to Brr6-yEGFP (*A*) and Brl1-yEGFP (*B*) in spite of their low expression levels (exposure time was 1 sec, and 488 nm illumination power was set to 100%). (*C*) dsRed-HDEL NE fiduciary marker is shown for comparison. Brl1 was found 3.3 nm deeper in the NE than Brr6 *(9)*. Scale bar: 2μm.

Influence of projection effects from 3D to 2D

Any 3D object tilted by an angle α appears shortened by a factor cos(α) when projected on the horizontal plane ('cosine effect', Fig. S5). Thus, distances measured by NuRIM tend to underestimate true 3D distances by a factor approximately equal to the average of cos(α). Our automated image analysis code preferentially recognizes well-contrasted NEs (associated with small projection angles), so if a nucleus is only cut in a grazing position by the focal plane, NuRIM does not produce statistics on it. The experimental average projection factor is therefore different than one would expect based on purely geometrical arguments.

In order to precisely estimate the projection factor, we performed *in silico* experiments. 2500 nuclei were generated where the radial position of NPCs was artificially shifted by 20 nanometers relative to the NE position. Correspondingly, NuRIM was applied to the simulated images and recovered a shift of 17.5 nm nanometers. Therefore, NuRIM correctively multiplies all values by a factor 20/17.5=1.14.

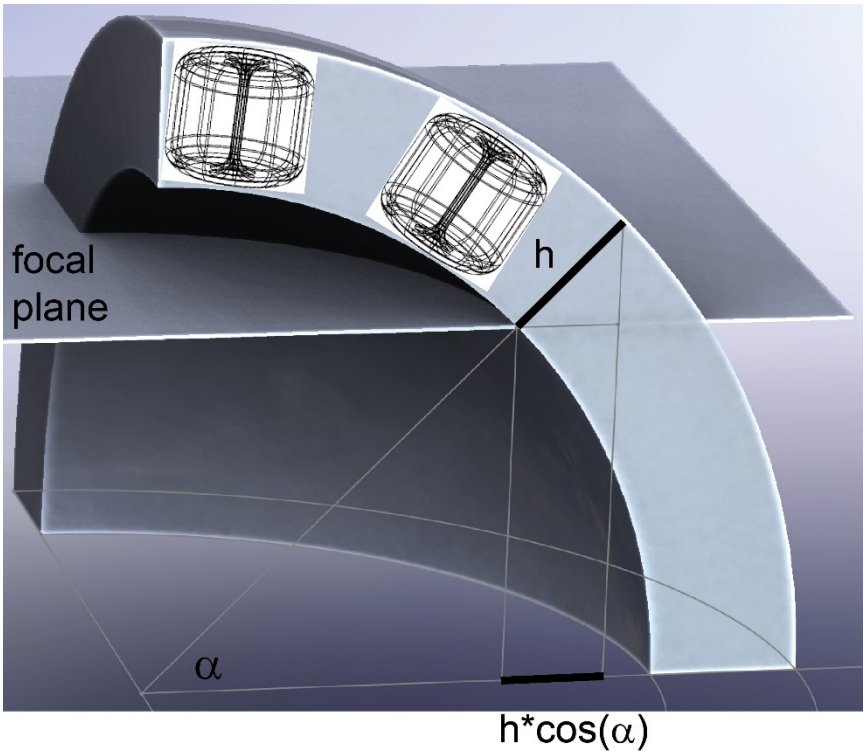

Fig. S5. Accounting for projections effects. The focal plane does not always cut the NE perpendicularly. Thus a true position difference equal to h in the NPC is only measured as h*cos(α) in the image plane. The precise value of the projection factor was determined on the basis of over 2500 simulated images, where h was set to 20 nm (*SI*, Dataset S1).

Recommendations on the use of NuRIM

It is essential to examine each image briefly to ensure that the image acquisition proceeded as planned, before attempting to analyze them.

We have insisted on using NuRIM as a differential method (i.e. one should only measure differences in positions, acquired under identical experimental conditions). When used in the recommended manner, an accuracy ~2 nm may be expected.

We have used an autofocus mechanism (PFS, Nikon) ensuring constant working distance between the coverslip and the microscope objective. In the absence of such a mechanism, each image should be adjusted for optimal focus by maximizing the apparent diameter across nuclei.

Our simulations as well as the results obtained with the NLS and NES strains show that NuRIM is quite resilient against high background fluorescence levels. We nonetheless recommend adopting a conservative approach when high backgrounds are present. In such cases, the "adjusted positions" (last column of the Excel tables produced by NuRIM) could differ from the experimental ones by more than 5 nm.

NuRIM includes a few dependencies on third-party code and libraries (e.g. the bio-format image library or utility functions such as "rdir" available on Matlab Central)(10, 11). These must be installed before NuRIM can be launched.

NuRIM was developed for images produced by our microscope. Differences in magnification and pixel size require minimal adaptations to our code

Table S1. Strains used for the present study

Strain	Genotype	Source
KWY165	MATa *leu2-3,112 trp1-1 can1-100 ura3-1 ade2-1 his3-11,15*	W303
KWY390	MATα leu2-3,112 trp1-1 can1-100 ura3-1 ade2-1 his3-11,15	W303
KWY6288	KWY390 TRP1::dsRed-HDEL	(1)
SWY1695	MATa ura3-1 his3-11,15 trp1-1 leu2-3,112 can1-100 ade2-1::ADE2:ura3 HIS3::GFP-NIC96	Bucci and Wente(12)
KWY8022	MATα ade2-1 NUP84-link-EGFP::CaURA3 TRP1::dsRed-HDEL HIS3:: cyc1-NLS-yEGFP	This study
KWY8023	MATα ade2-1 NUP84-link-EGFP::CaURA3 TRP1::dsRed-HDEL HIS3:: cyc1-NES-yEGFP	This study
KWY8024	MATα ade2-1 NUP159-link-GFP::CaURA3 TRP1:: dsRed-HDEL HIS3::cyc1-NLS-yEGFP	This study
KWY8025	MATα ade2-1 NUP159-link-GFP::CaURA3 TRP1:: dsRed-HDEL HIS3::cyc1-NES-yEGFP	This study
KWY6033	*KWY6288 NUP116-link-yEGFP::CaURA3*	(1)
KWY6034	*KWY6288 NUP100-link-yEGFP::CaURA3*	(1)
KWY6035	*KWY6288 NUP192-link-yEGFP::CaURA3*	(1)
KWY6036	*KWY6288 NUP157-link-yEGFP::CaURA3*	(1)
KWY6037	*KWY6288 NUP84-link-yEGFP::CaURA3*	(1)
KWY6038	*KWY6288 NUP85-link-yEGFP::CaURA3*	(1)
KWY6039	*KWY6288 NUP120-link-yEGFP::CaURA3*	(1)
KWY6040	*KWY6288 NUP170-link-yEGFP::CaURA3*	(1)
KWY6041	*KWY6288 NUP133-link-yEGFP::CaURA3*	(1)
KWY6042	*KWY6288 NUP145C-link-yEGFP::CaURA3*	(1)
KWY6043	*KWY6288 SEH1-link-yEGFP::CaURA3*	(1)
KWY6044	*KWY6288 POM34-link-yEGFP::CaURA3*	(1)
KWY6046	*KWY6288 NDC1-link-yEGFP::CaURA3*	(1)
KWY6048	*KWY6288 NUP82-link-yEGFP::CaURA3*	(1)

KWY6049	*KWY6288 NUP42-link-yEGFP::CaURA3*	(1)
KWY6051	*KWY6288 GLE1-link-yEGFP::CaURA3*	(1)
KWY6052	*KWY6288 NUP188-link-yEGFP::CaURA3*	(1)
KWY6053	*KWY6288 NUP60-link-yEGFP::CaURA3*	(1)
KWY6054	*KWY6288 NUP159-link-yEGFP::CaURA3*	(1)
KWY6562	*KWY6288 NIC96-link-yEGFP::CaURA3*	(1)
KWY6563	*KWY6288 NUP1-link-yEGFP::CaURA3*	(1)
KWY6564	*KWY6288 NUP53-link-yEGFP::CaURA3*	(1)
KWY6565	*KWY6288 NUP59-link-yEGFP::CaURA3*	(1)
KWY6567	*KWY6288 DBP5-link-yEGFP::CaURA3*	(1)
KWY6568	*KWY6288 KAP95-link-yEGFP::CaURA3*	(1)
KWY6569	*KWY6288 MEX67-link-yEGFP::CaURA3*	(1)
KWY6570	*KWY6288 MLP1-link-yEGFP::CaURA3*	(1)
KWY6571	*KWY6288 MLP2-link-yEGFP::CaURA3*	(1)
KWY6719	*KWY6288 NUP42-link-yEGFP::CaURA3 GLE1-link-yEGFP::HIS3MX*	(1)
KWY6717	*KWY6288 NUP120-link-yEGFP::CaURA3 GLE1-link-yEGFP::HIS3MX*	(1)
KWY6720	*KWY6288 MEX67-link-yEGFP::CaURA3 NUP133-link-yEGFP::HIS3MX*	(1)
KWY7506	*KWY6288 NUP84-longlink-yEGFP::CaURA3*	(1)
KWY7507	*KWY6288 NUP85-longlink-yEGFP::CaURA3*	(1)
KWY7508	*KWY6288 NUP120-longlink-yEGFP::CaURA3*	(1)
KWY7509	*KWY6288 NUP133-longlink-yEGFP::CaURA3*	(1)
KWY7510	*KWY6288 NIC96-longlink-yEGFP::CaURA3*	(1)
KWY8613	*KWY6288 HEH1-link-yEGFP::CaURA3*	This study
KWY8614	*KWY6288 HEH2-link-yEGFP::CaURA3*	This study
KWY8616	*KWY6288 yEGFP-NUP159::CaURA3*	This study
KWY8617	*KWY6288 yEGFP-NUP116::CaURA3*	This study
KWY8618	*MAT A/α leu2-3,112/leu2-3,112 can1-100/can1-100 ura3-1/ura3-1 ade2-1/ade2-1 his3-11,15/his3-11,15 GLE1-link-yEGFP::URA3/GLE1-link-yEGFP::HIS3MX TRP1::dsRed-HDEL/TRP1::dsRed-HDEL*	This study
KWY8619	*MAT A/α leu2-3,112/leu2-3,112 can1-100/can1-100 ura3-1/ura3-1 ade2-1/ade2-1 his3-11,15/his3-11,15 NUP133-link-yEGFP::URA3/NUP133-link-yEGFP::HIS3MX TRP1::dsRed-HDEL/TRP1::dsRed-HDEL*	This study
KWY8620	*MAT A/α leu2-3,112/leu2-3,112 can1-100/can1-100 ura3-1/ura3-1 ade2-1/ade2-1 his3-11,15/his3-11,15 NUP82-link-yEGFP::URA3/NUP82-link-yEGFP::HIS3MX TRP1::dsRed-HDEL/TRP1::dsRed-HDEL*	This study
KWY8621	*MAT A/α leu2-3,112/leu2-3,112 can1-100/can1-100 ura3-1/ura3-1 ade2-1/ade2-1 his3-11,15/his3-11,15 NUP170-link-yEGFP::URA3/NUP170-link-yEGFP::HIS3MX TRP1::dsRed-HDEL/TRP1::dsRed-HDEL*	This study
KWY7542	*MAT A his3-11,15 leu 2-3 trp 1-1 BRR6::BRR6-yEGFP-CaURA3 trp1::pADH1-dsRED-HDEL-TRP1*	
KWY7542	*MAT A his3-11,15 leu 2-3 BRL1::BRL1-yEGFP-CaURA3 trp1::pADH1-dsRED-HDEL-TRP1*	
KWY8611	*MATα leu2-3,112 can1-100 ade2-1 his3-11,15 KAP124-link-yEGFP::CaURA3 TRP1::dsRed-HDEL*	This study
KWY6896	*MAT A ade2-1::ADE2 ura3-1 leu2-3,112 trp1-1 his3-11,15 nup116ΔGLFGΔCTD(967-1113)-link-yEGFP::KANMX6 ZRP1::PADH1-dsRed-HDEL*	(13)
KWY6895	*MAT A ade2-1 ura3-1 his3-11,15 trp 1-1 leu2- 3,112 nup116ΔCTD-yEGFP nup116ΔCTD(967-1113)-link-yEGFP::KANMX6 TRP1::PADH1-dsRed-HDEL*	(13)

Table S2. Plasmids used in this study

Plasmid	Genotype	Reference

pKW1964	pFA6a-link-yEGFP-CaURA3	*(14)*
pKW1358	YIplac204-dsRed-HDEL	*(15)*
pKW2627	pGem-T_NatMx-RPL25NLS	*(1)*
pKW4421	pFA6a-longlink-yEGFP-CaURA3	*(1)*
pKW4422	pFA6a-link-superfolderGFP-CaURA3	*(1)*
pKW4423	pRS306-Nup157-yEGFP-CaURA3	*(1)*
pKW4424	pRS306-Nup170-yEGFP-CaURA3	*(1)*
pKW4425	pRS306-Nup188-yEGFP-CaURA3	*(1)*
pKW4426	pRS306-Nup192-yEGFP-CaURA3	*(1)*
pKW4588	pRS306-yEGFP-Nup116-CaURA3	This study
pKW4589	pRS306-yEGFP-Nup159-CaURA3	This study
pKW4589	pRS306-yEGFP-Nup159-CaURA3	This study

References

1. Rajoo S, Vallotton P, Onischenko E, & Weis K (2018) Stoichiometry and compositional plasticity of the yeast nuclear pore complex. *Proc Natl Acad Sci USA* 115(17):E3969-E3977.
2. Winey M, Yarar D, Giddings TH, & Mastronarde DN (1997) Nuclear pore complex number and distribution throughout the Saccharomyces cerevisiae cell cycle by three-dimensional reconstruction from electron micrographs of nuclear envelopes. *Mol Biol Cell* 8(11):2119-2132.
3. Pankajakshan P*, et al.* (2010) Point-Spread Function Model for Fluorescence Macroscopy Imaging. in *Conference Record of the Forty Fourth Asilomar Conference on Signals, Systems and Computers* (Asilomar), pp 1364-1368.
4. Hadjidemetriou S*, et al.* (2014) Detection and Tracking of Cell Divisions in Phase Contrast Video Microscopy. in *Third MICCAI Worshop on Microscopic Image Analysis with Applications in Biology*.
5. Digman MA, Wiseman PW, Choi C, Horwitz AR, & Gratton E (2009) Stoichiometry of molecular complexes at adhesions in living cells. *P Natl Acad Sci USA* 106(7):2170-2175.
6. Vallotton P (2008) Differential aberration correction (DAC) microscopy: a new molecular ruler. *Journal of Microscopy* 232(2):235-239.
7. Guizar M (2016) Efficient subpixel image registration by cross-correlation.
8. Wang R*, et al.* (2016) High resolution microscopy reveals the nuclear shape of budding yeast during cell cycle and in various biological states. *Journal of cell Science* 129:4480-4495.
9. Zhang WL*, et al.* (2018) Brr6 and Brl1 locate to nuclear pore complex assembly sites to promote their biogenesis. *J Cell Biol* 217(3):877-894.
10. D'Almeida F (2002) Fast 2D Max/Min Filter, 1.0.0.0.
11. Wetzler A (2018) Bresenham optimized for Matlab, 1.1.0.0.
12. Bucci M & Wente SR (1998) A novel fluorescence based genetic strategy identifies mutants of Saccharomyces cerevisiae defective for nuclear pore complex assembly. *Mol Biol Cell* 9:132a-132a.
13. Onischenko E*, et al.* (2017) Natively Unfolded FG Repeats Stabilize the Structure of the Nuclear Pore Complex. *Cell* 171(4):904-917.
14. Sheff MA & Thorn KS (2004) Optimized cassettes for fluorescent protein tagging in Saccharomyces cerevisiae. *Yeast* 21(8):661-670.

15. Bevis BJ, Hammond AT, Reinke CA, & Glick BS (2002) De novo formation of transitional ER sites and Golgi structures in Pichia pastoris. *Nat Cell Biol* 4(10):750-756.